Article

Current Biology

A Mechanical Feedback Restricts Sepal Growth and Shape in *Arabidopsis*

Highlights

- A stereotypical growth pattern generates tensile stress at the sepal tip
- A supracellular microtubule alignment forms along maximal tension at the sepal tip
- The strength of the mechanical feedback can modulate sepal shape
- The microtubule response to tension acts as an organ shape-sensing mechanism

Authors

Nathan Hervieux, Mathilde Dumond, Aleksandra Sapala, ..., Richard S. Smith, Arezki Boudaoud, Olivier Hamant

Correspondence

arezki.boudaoud@ens-lyon.fr (A.B.), olivier.hamant@ens-lyon.fr (O.H.)

In Brief

A key question in development is how organs know when to stop growing. Using the *Arabidopsis* sepal as a model, Hervieux et al. show that growth-derived mechanical stress impacts microtubule orientation at the sepal tip, further restricting growth in that domain. Such a mechanical feedback loop may constitute a general proprioception mechanism.

Hervieux et al., 2016, Current Biology *26*, 1019–1028
April 25, 2016
http://dx.doi.org/10.1016/j.cub.2016.03.004

CellPress

Current Biology
Article

A Mechanical Feedback Restricts Sepal Growth and Shape in *Arabidopsis*

Nathan Hervieux,[1] Mathilde Dumond,[1] Aleksandra Sapala,[2] Anne-Lise Routier-Kierzkowska,[2] Daniel Kierzkowski,[2] Adrienne H.K. Roeder,[3] Richard S. Smith,[2] Arezki Boudaoud,[1,*] and Olivier Hamant[1,*]
[1]Plant Reproduction and Development Laboratory, Université de Lyon, ENS Lyon, UCB Lyon 1, INRA, CNRS, 46 Allée d'Italie, 69007 Lyon, France
[2]Department of Comparative Development and Genetics, Max Planck Institute for Plant Breeding Research, Carl-von-Linné-Weg 10, 50829 Köln, Germany
[3]Weill Institute for Cell and Molecular Biology and Section of Plant Biology, School of Integrative Plant Sciences, Cornell University, Ithaca, NY 14853, USA
*Correspondence: arezki.boudaoud@ens-lyon.fr (A.B.), olivier.hamant@ens-lyon.fr (O.H.)
http://dx.doi.org/10.1016/j.cub.2016.03.004

SUMMARY

How organs reach their final shape is a central yet unresolved question in developmental biology. Here we investigate whether mechanical cues contribute to this process. We analyze the epidermal cells of the *Arabidopsis* sepal, focusing on cortical microtubule arrays, which align along maximal tensile stresses and restrict growth in that direction through their indirect impact on the mechanical anisotropy of cell walls. We find a good match between growth and microtubule orientation throughout most of the development of the sepal. However, at the sepal tip, where organ maturation initiates and growth slows down in later stages, microtubules remain in a configuration consistent with fast anisotropic growth, i.e., transverse, and the anisotropy of their arrays even increases. To understand this apparent paradox, we built a continuous mechanical model of a growing sepal. The model demonstrates that differential growth in the sepal can generate transverse tensile stress at the tip. Consistently, microtubules respond to mechanical perturbations and align along maximal tension at the sepal tip. Including this mechanical feedback in our growth model of the sepal, we predict an impact on sepal shape that is validated experimentally using mutants with either increased or decreased microtubule response to stress. Altogether, this suggests that a mechanical feedback loop, via microtubules acting both as stress sensor and growth regulator, channels the growth and shape of the sepal tip. We propose that this proprioception mechanism is a key step leading to growth arrest in the whole sepal in response to its own growth.

INTRODUCTION

A central and still unresolved question in developmental biology is how organs reach reproducible size and shape [1]. Evidence that organ size is controlled by intrinsic signals has been accumulating over the years. This was nicely demonstrated by Twitty and Schwind in 1931 [1]: grafting the limb bud from a large salamander onto a small salamander results in the growth of a large limb on a small salamander. In most organisms, including plants, the size and shape of organs is highly characteristic and varies little between individuals. In plants, evidence that organ size is tightly controlled is illustrated by the concept of compensation. Leaves with a reduced cell number can reach their normal size by increasing the rate or duration of the cell-expansion phase [2, 3]. However, the associated mechanisms are unknown. The control of organ size and shape involves the tight regulation of growth arrest, in addition to other variables, such as the number of cells recruited to the new organ primordium and the expansion and division rate of those cells. Although morphogen gradients are involved in the growing phase of organs, they have also been proposed to be involved in growth arrest: morphogens become diluted as growth occurs and, beyond a certain threshold of concentration, they may not promote growth anymore. This provides an interesting geometrical negative feedback loop in which shape and distance determine growth arrest [4–6].

Mechanical signals have been proposed to act as a means to inform the genetic control of development by providing a mechanism to probe an organ's developing size and shape (e.g., [7, 8]). In the wing imaginal disc of *Drosophila melanogaster*, cells grow uniformly despite the gradient of the growth-promoting factor Dpp emanating from the center of the disc [8–10]. A simple stress feedback on growth has been proposed to explain this disconnect between observed growth and the morphogens controlling it [8, 11, 12]. Dpp promotes growth of the central cells, causing compressive stresses locally, while also causing tensile stresses in the surrounding cells at the periphery of the disc. Beyond a certain threshold, compression is proposed to trigger an arrest of cell proliferation, whereas tensile stress enhances proliferation. The observed synchrony in cell division and growth in the wing disc is consistent with this hypothesis [8–11]. Yet, the role of mechanical forces in organ size is still debated. In particular, *dpp* concentration in the wing disc also scales with disc size [6], opening the possibility that both morphogen dilution and mechanical compression contribute to growth arrest.

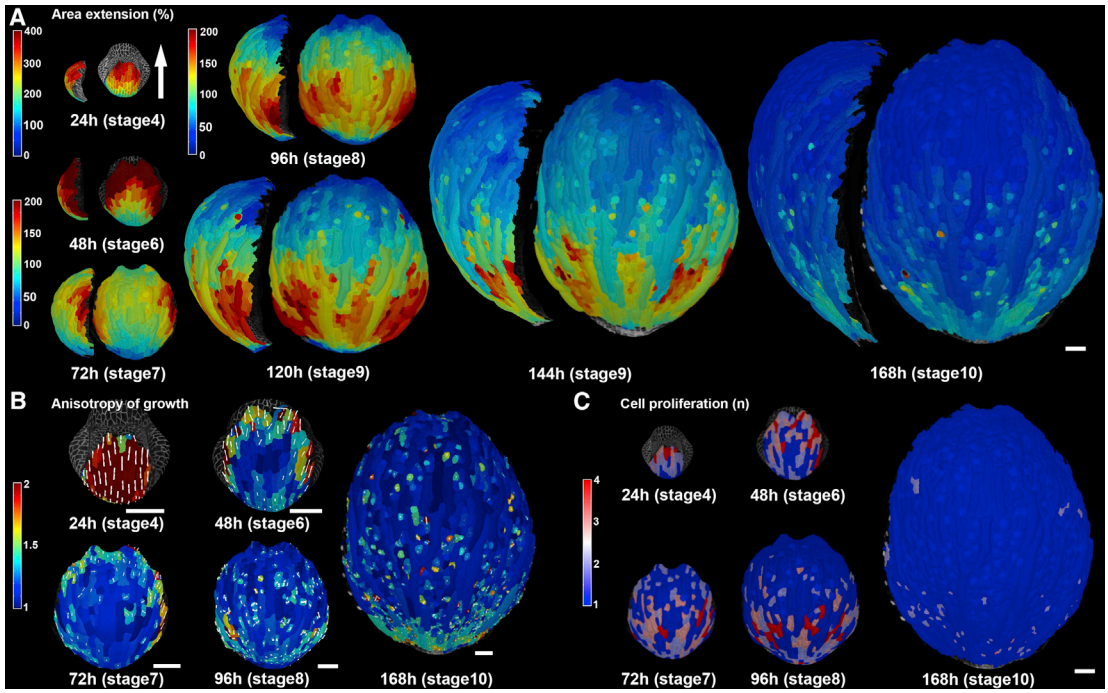

Figure 1. Growth Analysis for a Time-Lapse Series of an Abaxial Sepal Growing for 168 Hr

The white arrow shows the apicobasal axis of the sepal (the tip of the arrow corresponds to the distal tip of the sepal) for all images.

(A) Heatmap of areal expansion (%) over consecutive 24-hr intervals, displayed on the second time point (see also Figure S1). The developmental stage of the flower was assigned at each time point as in [22]. Each time point is displayed from the side (left) and from the top (right). The same magnification is used for all stages. Note that averaged growth data are represented: averaging is a similar approach to the Tauriello displacement field [21] and has a similar effect, i.e., smoothing out the noise to identify underlying trends.

(B and C) Images of selected time points from the image sequence displayed in (A).

(B) Anisotropy of growth calculated as deformation in maximal growth direction (PDG_{max}; PDG, principal direction of growth) divided by deformation in minimal growth direction (PDG_{min}). White bars represent the direction of maximal growth for cells displaying growth anisotropy above 20%.

(C) Cell proliferation over 24 hr displayed for selected time points.

Color scales indicate the number of daughter cells that arose from a single cell within the previous 24 hr. Scale bars, 50 μm. See also Figure S1.

In plants, mechanical stress and strain drive growth [13], providing a pervasive passive feedback on growth. The strongest evidence for active mechanical feedback in plants involves the cortical microtubules, which orient along maximal tensile stress directions [7, 14, 15]. Because the cortical microtubules guide the trajectories of cellulose synthase [16] that orient the deposition of cellulose microfibrils, this feedback directly controls the direction of maximal stiffness in cell walls [17, 18]. Cellulose restricts wall expansion in the direction of the microfibrils, and thus most likely plays a key role in growth arrest and in channeling final shape. An analysis of tension and microtubule patterns in the jigsaw-puzzle-shaped pavement cells supports such a scenario at the single-cell scale [19]. Using the *Arabidopsis* sepal as a model system, we show that this mechanism also operates at the organ level.

RESULTS

The Abaxial Sepal Exhibits a Stereotypical Growth Pattern

The sepal is the outermost organ in the flower; out of the four sepals in each flower, the abaxial sepal is the farthest from the stem axis. Because the final size and shape of this organ are relatively insensitive to environmental conditions, the contribution of intrinsic signals to its final shape can be analyzed more easily, making it an ideal system to investigate the role of mechanical signals in shaping organs.

To analyze cellular growth in the wild-type sepal, we performed time-lapse imaging of the abaxial sepal expressing a fluorescent plasma membrane marker. We used MorphoGraphX [20] to segment cells in the epidermis for each time point and analyze their growth properties. We chose 24-hr intervals, which reduced variability when compared with the 6-hr intervals reported previously [21]. A stereotypical pattern of growth could be observed (Figures 1A and 1B; Figure S1; n = 3 long time sequences). Using the staging defined in [22], we observed that, from the initiation of the primordium until stage 6, both growth rate (Figure 1A) and growth anisotropy (Figure 1B) were very high at the sepal tip and lower toward the base. The direction of maximal growth was along the longitudinal axis of the growing sepal (Figure 1B). Then, between stages 6 and 7, growth rates were greatly reduced at the sepal tip while maintaining a relatively fast anisotropic growth at the lateral margin. From stage 7, a region of isotropic, relatively fast growth appeared around the center of the sepal and gradually proceeded toward its base in later stages (Figure 1B). Cell proliferation followed global

gradients in growth rates as well as reflected the appearance of stomata lineages (Figure 1C).

The Tip of the Sepal Exhibits a Stereotypical Cortical Microtubule Pattern

To examine the molecular basis of this growth pattern, we next analyzed microtubule behavior during sepal growth. We used a transgenic line expressing both a membrane marker (LTI6b-2xmCherry) under the control of the UBQ10 promoter and a microtubule marker (GFP-MBD) under the control of the CaMV35S promoter.

As shown in other tissues (e.g., [18, 23, 24]), we found that the cortical microtubule (CMT) network is dynamic over time and space (Figure 2; Figure S2). We focused our analysis on regions and stages where the growth pattern exhibited marked changes in order to draw more clear-cut correlations. Before stage 6, CMT orientation was consistent over several cell files, perpendicular to the longitudinal axis of the sepal (Figures 2A–2C; $n > 10$). This orientation is also consistent with the predominant longitudinal growth direction at that stage (see Figure 1B), compatible with the role of CMTs in guiding cellulose deposition and thus in channeling growth direction. Then, at stage 7, when growth became more isotropic, we observed that the CMT network also became more isotropic (Figures 2D–2F; $n > 10$), again consistent with a scenario in which growth direction mainly depends on CMTs. At stage 9, the correlation between CMT orientation and growth was, however, only partially maintained (Figures 2G and 2H; $n > 10$): whereas isotropic growth in the center of the sepal correlated with isotropic CMT orientations (Figure 2J), CMTs in several cell layers at the slow isotropically growing tip were well aligned, tangentially to the sepal edge (Figure 2I). Importantly, microtubule arrays at the tip became more anisotropic, even though growth became slower and more isotropic (Figure 2K). Proximal and side views of growing sepals provided consistent patterns (Figures S2C and S2D).

It is well established that CMTs orient according to cell geometry, i.e., along the longitudinal axis of the cell, when growth stops in the hypocotyl [25]. Because CMTs remain predominantly transverse at the tip (Figure 2I), we next explored whether the CMT behavior at the tip may be better explained by a supracellular cue [7, 19, 26].

The Sepal Growth Pattern Prescribes a Mechanical Stress Pattern

Many supracellular cues may be involved in prescribing such a specific microtubule behavior at the sepal tip. Here we investigated whether growth-derived mechanical stress may be one of these cues. CMTs have indeed been found to orient along maximal tensile stress directions in the meristem, cotyledons, and immature seeds [7, 19, 27].

To test this hypothesis, we built a continuous two-dimensional mechanical model of the sepal that accounts for the surface walls of the epidermis and aimed at simulating stage 7 onward. The simulations were initialized with a half-disk shape. At a given time point, the system is assumed to be elastic and the elastic modulus increases from the base to the tip of the sepal so as to mimic stiffening associated with maturation; because we observed a sharp decay in growth rate at the tip of sepals from stage 8 onward, we assumed the extent of the gradient to be larger than the initial size of the simulated sepal and the increase in stiffness to be 10-fold. The base of the sepal is fixed and turgor pressure is applied perpendicularly to the remainder of the boundary; equilibrium displacements are computed using the finite element method (for details, see Experimental Procedures), yielding an equilibrium shape with a greater area than the initial shape. Growth is modeled incrementally: the equilibrium shape of the previous step is taken in the following step as the initial shape to which turgor is applied again [5]. This leads to a succession of configurations with increasing area (Figure 2L), simulating sepal growth. As expected from the gradient in stiffness [13, 28], we observed a distal region with reduced growth rates and that covered more and more of the simulated sepal (Figure 2L). Because spatial differences in growth rate can induce mechanical stress, we examined the orientation of the main stress (Figure 2M) and found a pattern of transverse tensile stress at the proximal part of the stiff region.

To test whether the emergence of such a stress pattern depends on the model design, we also developed a model variant in which elastic properties are constant over the whole sepal and differential growth is instead implemented by a gradient in plastic properties. The corresponding simulations provided qualitatively similar results, i.e., transverse tensile stress at the border between the more or less plastic regions (Figures S3B and S3C).

These results thus provide a scenario in which a growth gradient can generate transverse tensile stress at the border between the two growing domains. In turn, these stresses may coordinate cell behavior. Interestingly, this predicted pattern of stress matches the transverse orientation of CMTs at the sepal tip (see Figures 2G, 2I, and 2K). Therefore, these data are consistent with the following scenario: first, CMTs channel the sepal growth direction; then, as a growth gradient appears, tensile stresses are building up at the tip of the sepal, which in turn would lock the CMTs in a tangential orientation at the tip, restricting radial growth of the sepal at the tip.

CMTs Align along Maximal Tensile Stress in Growing Sepals

To test this hypothesis, we performed mechanical perturbations and checked whether CMTs would align along the new stress pattern.

First, we performed compression experiments. Young floral buds were placed under a coverslip for 3 hr and microtubule orientation was recorded before and after compression (Figures 3A–3I; $n = 6$). As observed in cotyledons with the same setup [19], we found that CMTs became hyper-bundled in the compressed part of the sepal (Figure 3E), whereas CMTs in the non-compressed sides of the sepal seemed unaffected (Figure 3F). The response was reversible, demonstrating that the microtubule hyper-bundling response was not caused by cell death (Figure 3H).

To further test the impact of mechanical stress on sepal shape, we next induced a transient phase of isotropic growth by depolymerizing CMTs in the sepal and observed the resulting sepal shape and microtubule behavior. We reasoned that such a treatment should enhance growth rate in the sepal transverse direction, when compared to the untreated sepal, and thus the anisotropy and magnitude of mechanical stress at the tip.

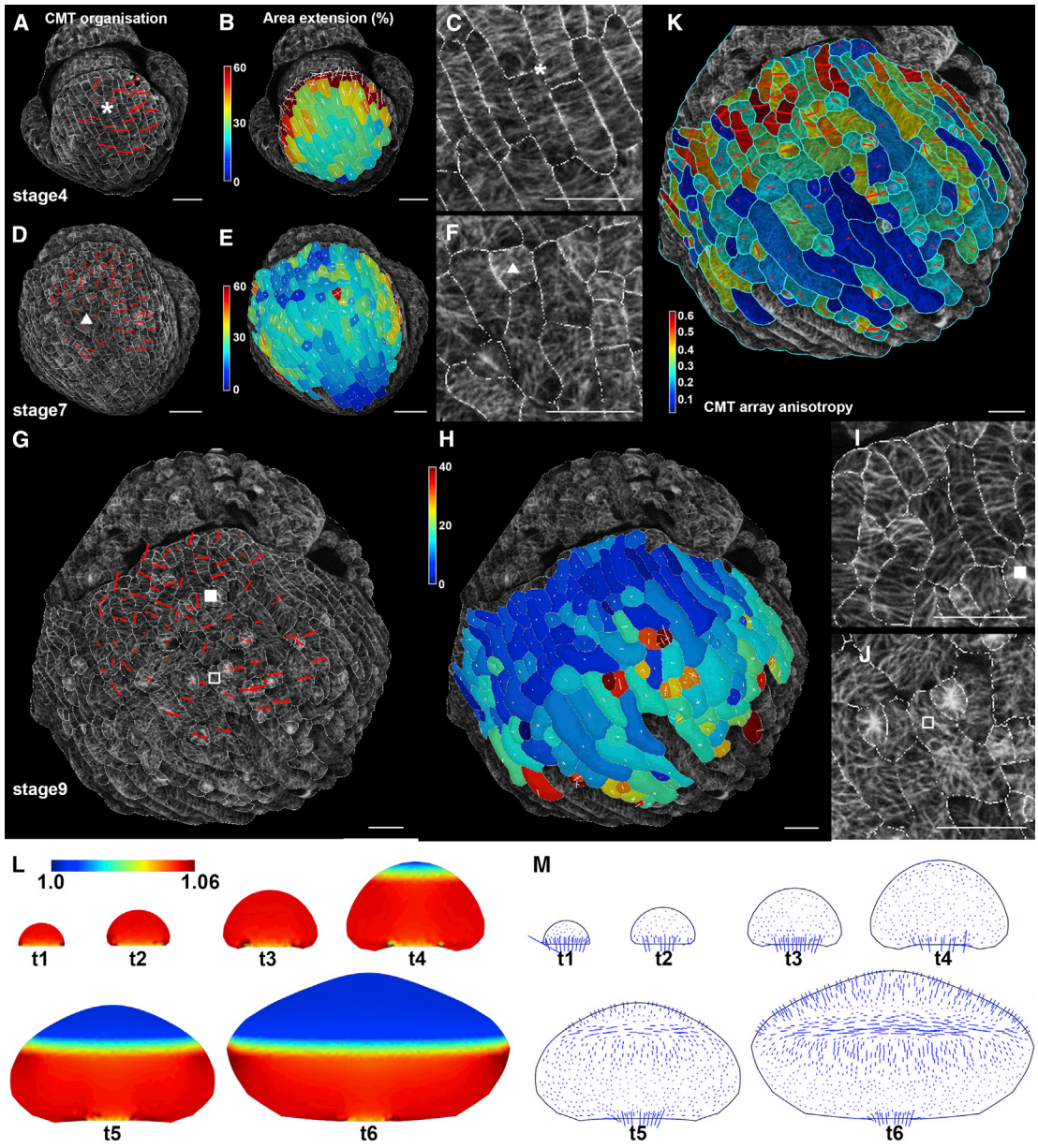

Figure 2. A Stereotypical Growth and Cortical Microtubule Pattern Prescribed a Mechanical Stress Pattern at the Tip

(A, D, and G) CMT organization at the surface of the abaxial sepal (see also Figure S2). The direction and length of the red bars indicate the average orientation and anisotropy of CMTs in each cell, respectively.

(B, E, and H) Heatmap of areal expansion (%) over 24-hr intervals displayed on the first time point. PDGs are indicated in white for expansion and in red for shrinkage.

(C, F, I, and J) Details of CMT organization in regions highlighted with a white symbol in (A), (D), and (G).

(K) Heatmap of the anisotropy of CMT arrays presented in (G).

(L and M) Mechanical simulation of a growing sepal (successive time points), without any mechanical feedback. Areal growth rates (L) as well as stress direction and magnitude (M) are represented.

Scale bars, 20 μm. Scale is identical for all time points in the simulation. See also Figure S2.

Sepals were treated with 20 μg/ml oryzalin for 3 hr, and this was sufficient to deplete most of the microtubules for a period of 24 hr (Figures 3J–3N; n = 10). As observed in the shoot apical meristem, this did not impact the pattern of growth rate [7]: the tip of the sepal still experienced slow growth after oryzalin treatment (Figure 3M). As expected, oryzalin treatment also amplified growth isotropy in the sepal (Figures 3K and 3M). CMTs did repolymerize in this context, and the first aligned CMT arrays could be observed 48 hr after oryzalin treatment. Strikingly, CMTs followed a clear-cut supracellular alignment at the tip and isotropic orientations in the center of the sepal (Figure 3N), matching the predicted pattern of stress.

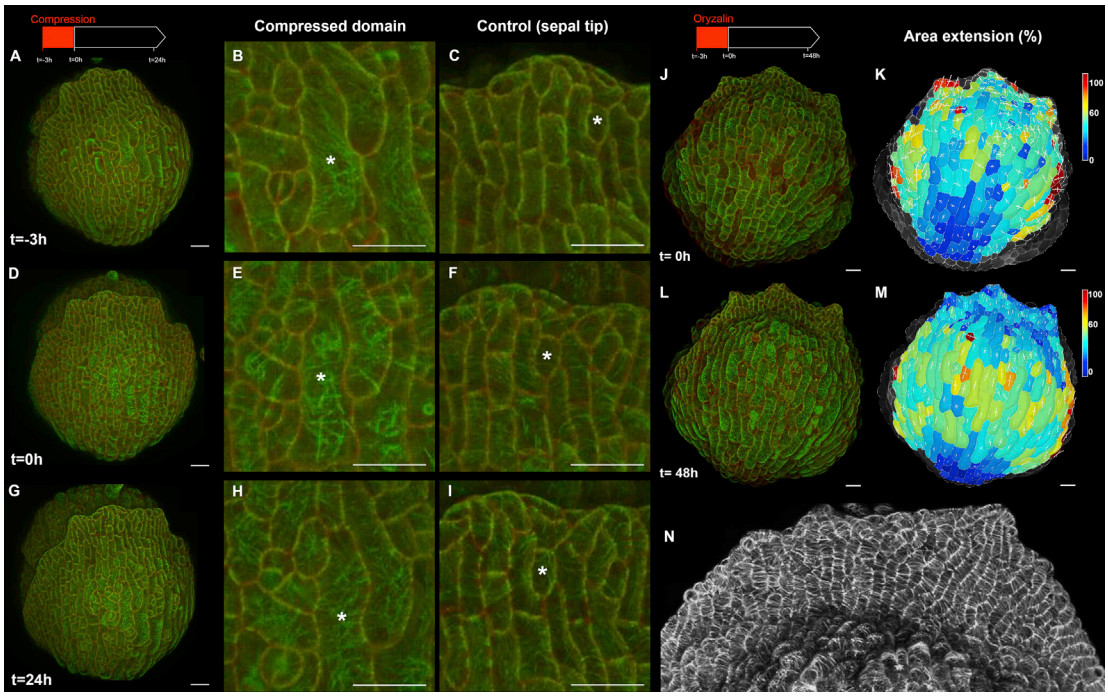

Figure 3. CMTs Align along Maximal Tensile Stress in Growing Sepals

(A–I) Compression of the abaxial sepal results in the reversible apparent bundling of CMTs. A white asterisk is added to help in the observation of the cell lineage in the different time points.

(A, D, and G) Live imaging of an abaxial sepal before (A) and after compression (D and G).

(B, E, and H) Close-up of the CMT apparent bundling response in the compressed domain.

(C, F, and I) Close-up of CMT behavior in the uncompressed domain (control).

(J–N) Effect of oryzalin treatment on CMT orientation and growth pattern.

(J and L) Live imaging of an abaxial sepal after oryzalin treatment.

(K and M) Heatmap of areal expansion (%) over 24-hr intervals displayed on the first time point. PDGs are indicated with expansion in white and shrinkage in red.

(N) Close-up of the tip of an abaxial sepal 48 hr after oryzalin treatment showing a supracellular CMT alignment at the tip.

Scale bars, 20 μm. See also Figure S3.

Altogether, these data are consistent with CMTs aligning with maximal tensile stress in the sepal, as shown in other tissues. A scenario in which CMTs align at the sepal tip along growth-derived stress is thus plausible.

A Mechanical Feedback May Channel Sepal Shape

To test whether such a mechanical feedback would be sufficient to affect sepal shape, we incorporated this hypothesis into our sepal growth model. Because of the similarities between the plastic and elastic model presented above, in the following we concentrated our efforts on the growth model that is based on a gradient of elastic properties. We assumed the material to be mechanically anisotropic, so as to represent the anisotropy of cellulose arrays in the cell wall, high anisotropy corresponding to high alignment of cellulose microfibrils and the orientation of the stiffest direction corresponding to the main orientation of microfibrils. In order to account for the orientation of CMTs according to stress and the subsequent cellulose synthesis, we assumed that, at each step, the stiffest direction aligns with the direction of maximal stress in the previous step, and that the level of mechanical anisotropy is an increasing Hill-like function of the stress anisotropy (Figure S3A; see Experimental Procedures); the level of feedback can be modulated through the two parameters of this Hill function (sharpness s of response and maximal response α_M). We found that moderate levels of feedback yielded unstable, noisy sepal shapes, consistent with the growth heterogeneity observed in a cellular model with similar hypotheses [29]. Because CMTs exhibit supracellular patterns, we reasoned that such a feedback would contribute to sepal shape only if microtubules primarily respond to the stronger supracellular stress pattern, and less to the local stress pattern, as shown previously in cotyledons [19]. Therefore, we assumed that mechanical anisotropy depends on the stress field averaged over the whole sepal. Such spatial averaging may reflect the time it takes for the wall mechanical anisotropy to change, and would also account for the stabilization of microtubule orientation by tension [7, 19]. This yielded more-regular shapes. In all cases, mechanical stress was transverse at the proximal part of the slowly growing region, close to the front with the fast-growing region (Figures 4B, 4E, and 4H). Promoting feedback strength led to increased mechanical anisotropy in the transverse orientation in the upper part of the sepal (Figures 4C, 4F, and 4I). As feedback strength increased, we found that the tip became more and more triangular (Figures 4A, 4D, and 4G; see Figure 2L for no feedback at all). For higher feedback level, we found that the tip was sharper and the sepal was narrower

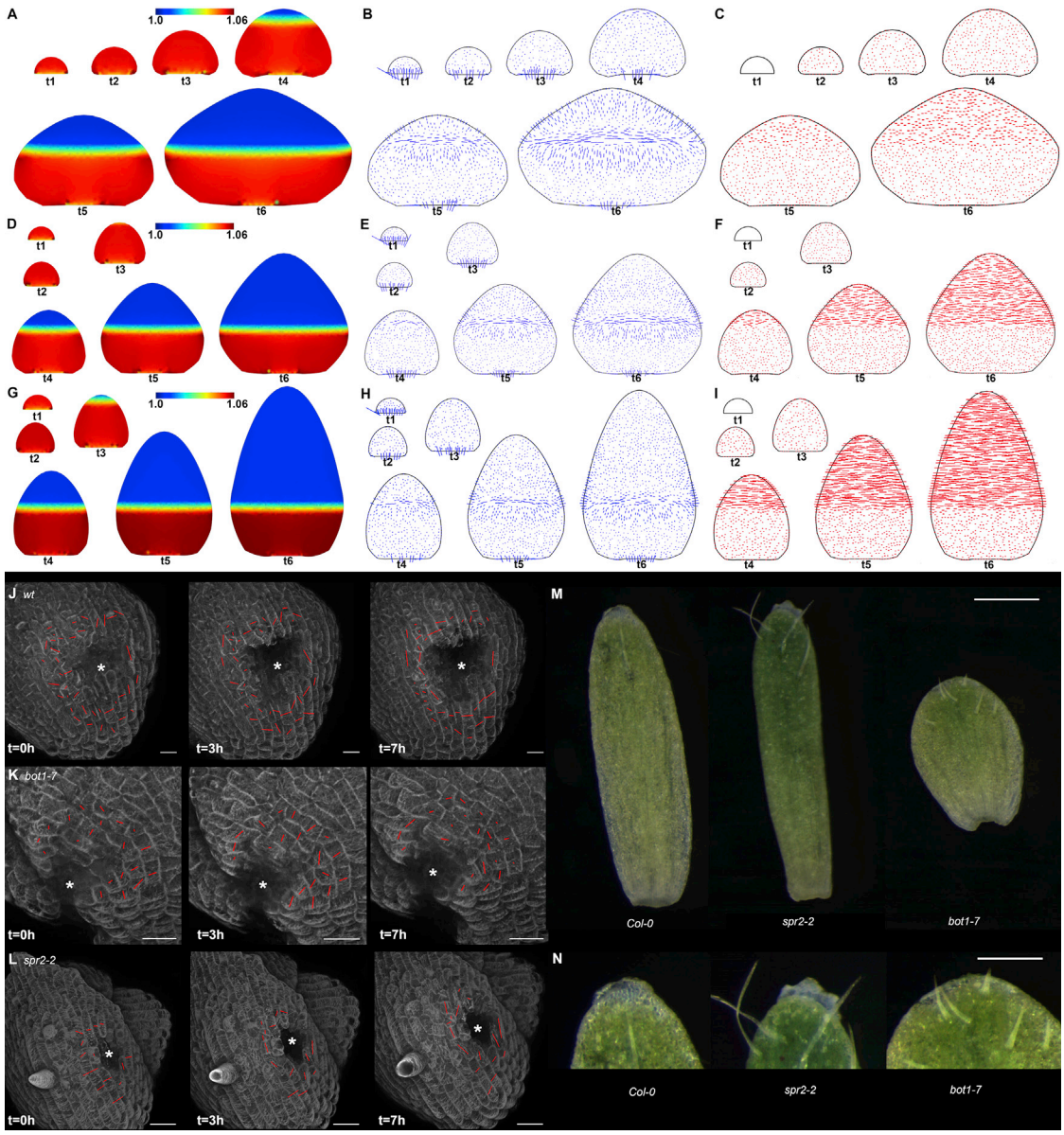

Figure 4. A Mechanical Feedback May Channel Sepal Shape

(A–C) Mechanical simulation of a growing sepal, with a weak mechanical feedback on growth direction ($s = 6$, $\alpha_M = 2$). The areal growth rate (A), stress direction and magnitude (B), and resulting mechanical anisotropy (C) are represented. The scale is identical for all time points.

(D–F) Mechanical simulation of a growing sepal, with a moderate mechanical feedback on growth direction ($s = 20$, $\alpha_M = 2$). The areal growth rate (D), stress direction and magnitude (E), and resulting mechanical anisotropy (F) are represented. The scale is identical for all time points.

(G–I) Mechanical simulation of a growing sepal, with a strong mechanical feedback on growth direction ($s = 20$, $\alpha_M = 3.5$). The areal growth rate (G), stress direction and magnitude (H), and resulting mechanical anisotropy (I) are represented. The scale is identical for all time points.

(J–L) Live imaging of the CMT response after mechanical ablation in different genotypes.

(J) Ablation induces a circumferential orientation of microtubule arrays around the site of ablation in the WT.

(K) The CMT response to ablation is slower in the *botero1-7* mutant.

(L) The CMT response to ablation occurs earlier in the *spiral2-2* mutant: a full CMT reorientation was visible as early as 3 hr after ablation.

The direction and length of the red bars indicate the average orientation and anisotropy of CMTs in each cell, respectively. Asterisks indicate the ablation sites. Scale bars, 20 μm.

(M) Mature sepals in the wild-type (Col-0) and *botero1-7* and *spiral2-2* mutants. Scale bar, 1 mm.

(N) Close-up of the tip of mature sepals in the corresponding genotype. Scale bar, 0.5 mm.

See also Figure S4.

(Figure 4G). The predicted pattern of mechanical anisotropy is comparable to observed CMT alignment at the very tip of the sepal, when a sharp growth gradient appears with the tip slowing down its growth (see Figures 2G–2I). At later stages, however, the CMT pattern looks more heterogeneous. Such noisy patterns may in part reflect local heterogeneities in growth rates, and thus in mechanical stress.

To check whether the main conclusion from the simulations depends on the choice of parameters, we tested different types of gradients in model variants: a larger linear gradient, a quadratic gradient, a sigmoid gradient, and a double gradient were implemented and, although the simulations provided quantitatively different results, they were all qualitatively similar: when the feedback strength increased, the tip became more triangular and the sepal became narrower (Figure S3). Altogether, this confirms that growth-derived stress may impact sepal shape.

To test these conclusions experimentally, we used two mutants impaired in microtubule dynamics to modify the response of the sepal cells to mechanical perturbations. The CMT response to stress depends on katanin-driven microtubule-severing activity [19, 29]. First, we verified that mutants with reduced microtubule-severing activity slowed down their CMT response to mechanical stress in the sepal. To do so, we performed large-scale ablations in the *bot1-7* katanin allele. As expected, a circumferential reorientation of the CMTs could be detected 3 hr after ablation in the WT (Figure 4J; $n > 10$; Figure S4A), whereas the CMT reorientation was slower and less obvious in the *bot1-7* mutant (Figure 4K; $n > 10$). To further test the conclusions of the model, we also required a mutant with an increased microtubule response to mechanical stress. SPIRAL2/TORTIFOLIA was proposed to prevent microtubule severing at the site of crossing over [30–32]; thus, in a *spr2* mutant, we would expect an enhanced response to mechanical perturbations because microtubule severing and dynamics are promoted. As predicted, CMT arrays were oriented circumferentially around the ablation in *spr2-2*. Interestingly, this happened earlier than in the WT, as full CMT reorientation was accomplished as early as 3 hr after ablation (Figure 4L; $n = 8$). Note that cells with well-aligned CMTs tend to reorient their CMT arrays more slowly than cells with more random CMT orientations in the wild-type, consistent with the promotion of CMT reorganization by crossovers (see, e.g., [33–36]). This differential response was observed in response to mechanical perturbations in meristematic cells with different microtubule patterns before ablation [29]. Although CMTs were well aligned in all cells of the *spr2-2* sepals before ablation (Figure 4L, left panel), CMTs still reoriented faster than the wild-type, thus further confirming that this mutant exhibits an increased microtubule response to mechanical stress. Altogether, this provides a series of genotypes in which the effects of an enhanced (*spr2-2*) or reduced (*bot1-7*) mechanical feedback on CMTs can be analyzed.

We also noticed that the sepal shapes of *bot1-7* and *spr2-2* seem to support our model's prediction that modulating the response of CMTs to mechanical stress should affect the final shape of the tip (Figures 4M and 4N; $n > 10$). Whereas the tip was smooth and rounded in *bot1-7*, the tip of *spr2-2* sepals formed triangular shapes, which is consistent with a hyper-response of CMTs at the tip, as predicted by our model (compare Figures 4A, 4D, and 4G with Figures 4M and 4N).

We also observed that *spr2-2* sepals were narrower than *bot1-7*. Although this is consistent with our model predictions, because of the complexity and heterogeneity of such a large tissue, it is likely that other players are also involved. In particular, in addition to the regulators of cellulose deposition and associated mechanical feedback, sepal shape also relies on large-scale biochemical gradients. Although the presence of a genetic "polarizer" remains to be formally demonstrated in such tissues [37, 38], it may add another layer of complexity to this picture, potentially adding robustness to sepal shapes in parallel to the mechanical feedback described here (Figures S4B–S4D). Altogether, our results show that the modulation of the microtubule response to mechanical stress can affect the shape of the sepal tip, consistent with a role of mechanical signals in channeling organ shape.

DISCUSSION

Our study suggests that differential growth during sepal development generates a stress pattern that feeds back on CMT orientation and further channels the growth pattern, notably at the sepal tip. Albeit at a different scale, this result echoes work conducted on shoot apical meristems where it was shown that differential growth between adjacent cells also generates mechanical conflicts that in turn further promote the maintenance of growth heterogeneity and the competence to generate marked differential growth during organogenesis [29]. We propose that the microtubule-tension feedback operating at the tip of the sepal functions as a shape-sensing mechanism: by resisting tangential tension, microtubules hinder further transverse expansion of the sepal; this may be the first step leading to growth arrest at the tip. Interestingly, in the shoot meristem, the domain that exhibits such a strong supracellular microtubule alignment is predicted to be under high tensile stresses. In that domain, cells grow at a very low rate and mostly in the direction of maximal stress [39], consistent with a scenario in which cells end up reducing their growth by resisting the increasing maximal stress.

Note that we considered the growth of the abaxial sepal independent of the contact of its neighbors. It is possible that other organs within the flower, and most notably the opposing adaxial sepal, add another mechanical input, by further restricting the expansion of the abaxial sepal. This type of mechanical constraint within the developing leaf bud was proposed to play a role in shaping folded leaves [40–42].

There is now accumulating evidence that mechanical signals play a key role in controlling cell division, cell polarity, and cell fate in animal single cells [43–49]. This also implies that mechanical signals largely contribute to shaping individual cells. Although this remains to be fully shown, mechanical signals also seem to shape plant cells (e.g., [19, 50]). The contribution of mechanical signals in shaping multicellular objects is more difficult to tackle because of the added complexity, notably in animal tissues where cells can migrate/intercalate, and because growth can be very fast during the main morphogenetic events of embryogenesis. Yet, mechanical forces have been involved in promoting major multicellular shape changes, notably in *Drosophila* [51–54], *Ciona* [55], zebrafish [56, 57], and *Caenorhabditis* [58]. However, the role of forces in tissues does not

seem to be restricted to the channeling of existing morphogenetic events, as they have been proposed to trigger growth arrest through their shape-sensing role [8, 9, 11] and even to initiate major developmental steps, such as mesoderm differentiation [56, 59, 60]. Here we take advantage of the relatively simpler mechanics of plant tissues to show that supracellular mechanical signals do contribute to the formation of organs with consistent shapes, through a microtubule-based growth restriction process and in parallel to morphogens, despite heterogeneity at the individual-cell level. As shown for organ polarity in which mechanical stress has been involved both in plants and animals [5, 53], we thus propose that mechanical signals act as organ shape-sensing factors across kingdoms, triggering growth arrest and generating organs with reproducible shapes.

EXPERIMENTAL PROCEDURES

Plant Material and Growth Conditions

For growth analysis, we used the *pUBQ10::myrYFP* line kindly provided by Raymond Wightman. In this line, myrYFP corresponds to a YFP that is N-terminally modified with a short peptide that is myristoylated and probably acylated (R. Wightman, personal communication). Plants were grown under long-day conditions [61]. *p35S::GFP-MBD* (WS-4) and *p35S::GFP-TUA6* were described previously [7, 62]. The membrane reporter line *pUQ10::Lti6b-2xmCherry* (Col-0) was kindly provided by Yvon Jaillais. The *botero1-7* katanin mutant allele was previously isolated [63] and described [29]. The *spiral2-2* mutant allele was previously described [31]. For mechanical perturbations and microtubule alignment analysis, plants were grown on soil in a phytotron under short-day conditions (8 hr/16 hr light/dark period) for 4 weeks and then transferred to long-day conditions (16 hr/8 hr light/dark period).

Live Imaging of the Growing Abaxial Sepal

One- to 2-cm-long main inflorescence stems were cut from the plant. To access young buds, the first 10–15 flowers were dissected out and the stem was then kept in an apex culture medium [64] supplemented with 6-benzylaminopurine (900 μg/L). Twenty-four hours after dissection, the young buds were imaged with an SP8 laser-scanning confocal microscope (Leica) using long-distance 25× (NA 0.95) or 40× (NA 0.8) water-dipping objectives. During time-lapse imaging, plants were kept in one-half MS medium [61] and imaged every 24 hr for up to 8 days. Flowers were dissected at the end of the time-lapse series to determine their growth stage based on internal organs [22].

Mechanical Perturbations

All experiments were performed on dissected apices as described above. Ablations were performed manually using a small needle, as in [29]. Compression was achieved by placing a coverslip on top of the flower for 3 hr; the coverslip was then removed carefully for imaging as in [19]. Oryzalin treatment was achieved by immersing dissected plants in an aqueous solution containing oryzalin at 20 μg/ml for 3 hr and then washing twice with water, as in [7].

Image Analysis

Images were processed with MorphoGraphX 3D image analysis software [20]. Stages of flower growth were determined in the time-lapse series using MorphoGraphX clipping planes to examine internal organs in cross-section. For better visualization of the general growth patterns, the areal growth maps displayed in Figure 1 show the growth averaged for each cell and its immediate neighbors, weighted by cell area.

Computational Modeling

We built a continuous mechanical model for sepal morphogenesis, starting from a model previously developed for fission yeast [65]. Only surface cell walls are modeled, yielding a two-dimensional medium with a prescribed distribution of mechanical properties. Morphogenesis occurs by successive increments in area: the rest shape at step n is inflated by turgor pressure, P, leading to a new equilibrium shape, which is then used as a rest shape for the next step, $n + 1$. At each step, the equilibrium configuration is found using the finite element method and the sepal is remeshed so as to keep a roughly constant mesh size. The model was implemented in freefem++ [66], and the results were analyzed using Python scripts. In the present study, we accounted for three new ingredients: mechanical anisotropy, mechanical feedback, and the gradient in mechanical properties, as detailed hereafter.

Mechanical anisotropy was introduced to account for cellulose fibrils locally more oriented in direction a; the coordinate system (a, b) may vary spatially. We used the generalized Hooke's law linking the stress tensor σ and the strain tensor ε through the elasticity matrix C^1,

$$\begin{pmatrix}\sigma_{aa}\\ \sigma_{bb}\\ \sigma_{ab}\end{pmatrix} = C^1\begin{pmatrix}\varepsilon_{aa}\\ \varepsilon_{bb}\\ \varepsilon_{ab}\end{pmatrix},\ C^1 = \begin{pmatrix}A_1 & B & 0\\ B & A_2 & 0\\ 0 & 0 & C\end{pmatrix},$$

where $A_1 = (1-\nu)E/((1+\nu)(1-2\nu))(1+\alpha/2)$, $A_2 = (1-\nu)E/((1+\nu)(1-2\nu))(1-\alpha/2)$, $B = \beta\sqrt{A_1A_2}$, and $C = E/(1+\nu)$, E being the reduced elastic modulus, ν the reduced Poisson's ratio, α the mechanical anisotropy, and β a non-dimensional modulus ($\beta < 1$ for the elasticity matrix to be well defined). Note that $A_1 > A_2$, meaning that direction a is stiffer than direction b, consistent with the mean orientation of cellulose microfibrils.

To incorporate the mechanical feedback, we first compute the eigenvalues (σ_1 and σ_2, $\sigma_1 > \sigma_2$) and corresponding eigenvectors (v_1 and v_2) of the stress tensor. In the next step, we set direction $a = v_1$ and the mechanical anisotropy $\alpha = 2\alpha_M/[1+\exp[-s(\sigma_1-\sigma_2)/(\sigma_1+\sigma_2)]] - \alpha_M$. These two equations are similar to previous work [67]. They mean that the next-stiffest direction matches the maximal stress orientation, whereas anisotropy varies between 0 for isotropic stress and its maximal value α_M when the stress is highly anisotropic; s quantifies the steepness of the response to stress.

The starting configuration is always a semi-disk of radius 1.1. In order to account for the observed growth gradient at later stages, we assume a low value of modulus, $E = Y_m E$, in the proximal region delimited by a line at a distance d_m from the sepal basis, a high value of the modulus, $E = Y_M E$, in the distal region delimited by a line at a distance d_M from the sepal basis, and a distance-based linear interpolation of the two values of modulus between these two lines.

We also tested quadratic and sigmoid interpolations of the two values of the modulus, as well as the use of two linear elasticity gradients, with the second one remaining at the tip of the sepal ($d^1{}_m = 3$, $d^1{}_M = 4$, $d^2{}_m = 2$ from the tip, $d^2{}_M = 1$ from the tip, $Y^1 = 0.1$ at the bottom, $Y^2 = 0.5$ in the middle, $Y^3 = 1$ at the tip). We also considered the possibility of a molecular polarizer biasing growth toward the longitudinal direction in the proximal region, i.e., before the elasticity gradient. We defined a new elasticity matrix C^2 in addition to the previously defined C^1, with parameters $E = 3.27$ MPa and $A_1 - A_2 = 0.6$ MPa, and a new parameter γ, such that $C = (1-\gamma)C^1 + \gamma C^2$. (Thus, γ represents the relative strength of the molecular polarizer.) $\gamma_1 = 0.75$ in the proximal region and $\gamma_2 = 0$ in the distal region. To test whether the observed shapes were due to the artificial increase of the modulus, we also implemented a version where the observed growth gradient was reproduced through differential plasticity (at each time step, a fraction p of the displacement field is kept as a permanent deformation accounting for growth), with no elasticity gradient, where $p_m = 1$ and $p_M = 0.1$.

In the simulations shown here, we used $p = 0.5$ MPa, $E = 3.27$ MPa, $\nu = 0.48$, $\beta = 0.5$, $\alpha_M = 2$ or 3.5, $s = 6$ or 20, $Y_m = 0.1$, $Y_M = 1$, $d_m = 3$, $d_M = 4$, and $d_m = 1$, $d_M = 5$ to test for longer gradient. The dimensionless size of the mesh was 1/5. In addition, we explored a range of other values and found the same qualitative results.

SUPPLEMENTAL INFORMATION

Supplemental Information includes four figures and can be found with this article online at http://dx.doi.org/10.1016/j.cub.2016.03.004.

AUTHOR CONTRIBUTIONS

N.H., A.-L.R.-K., and D.K. performed the biological experiments. N.H., A.S., and A.-L.R.-K. carried out the image analysis. M.D. carried out numerical simulations. N.H., M.D., A.H.K.R., R.S.S., A.B., and O.H. designed the study. N.H., M.D., and O.H. wrote the manuscript, with contributions from all co-authors.

ACKNOWLEDGMENTS

This work was supported by Human Frontier Science Program grant RGP0008/2013, the European Research Council (ERC-2013-CoG-615739 "MechanoDevo"), and DFG grant SFB 680. We thank Ray Wightman and Yvon Jaillais for sharing unpublished material and Miltos Tsiantis for offering the help of D.K. to this work. We also thank our HFSP collaborators, Lilan Hong, Mingyuan Zhu, Hagen Reinhardt, Tamiki Komatsuzaki, Chun-Biu Li, and Satoru Tsugawa for helpful discussions and critical reading of this manuscript.

Received: November 19, 2015
Revised: February 9, 2016
Accepted: March 1, 2016
Published: April 14, 2016

REFERENCES

1. Vogel, G. (2013). Mysteries of development. How do organs know when they have reached the right size? Science *340*, 1156–1157.
2. Horiguchi, G., Ferjani, A., Fujikura, U., and Tsukaya, H. (2006). Coordination of cell proliferation and cell expansion in the control of leaf size in *Arabidopsis thaliana*. J. Plant Res. *119*, 37–42.
3. Hisanaga, T., Kawade, K., and Tsukaya, H. (2015). Compensation: a key to clarifying the organ-level regulation of lateral organ size in plants. J. Exp. Bot. *66*, 1055–1063.
4. Jaeger, J., Irons, D., and Monk, N. (2008). Regulative feedback in pattern formation: towards a general relativistic theory of positional information. Development *135*, 3175–3183.
5. Kuchen, E.E., Fox, S., de Reuille, P.B., Kennaway, R., Bensmihen, S., Avondo, J., Calder, G.M., Southam, P., Robinson, S., Bangham, A., and Coen, E. (2012). Generation of leaf shape through early patterns of growth and tissue polarity. Science *335*, 1092–1096.
6. Wartlick, O., Mumcu, P., Kicheva, A., Bittig, T., Seum, C., Jülicher, F., and González-Gaitán, M. (2011). Dynamics of Dpp signaling and proliferation control. Science *331*, 1154–1159.
7. Hamant, O., Heisler, M.G., Jönsson, H., Krupinski, P., Uyttewaal, M., Bokov, P., Corson, F., Sahlin, P., Boudaoud, A., Meyerowitz, E.M., et al. (2008). Developmental patterning by mechanical signals in *Arabidopsis*. Science *322*, 1650–1655.
8. Shraiman, B.I. (2005). Mechanical feedback as a possible regulator of tissue growth. Proc. Natl. Acad. Sci. USA *102*, 3318–3323.
9. Hufnagel, L., Teleman, A.A., Rouault, H., Cohen, S.M., and Shraiman, B.I. (2007). On the mechanism of wing size determination in fly development. Proc. Natl. Acad. Sci. USA *104*, 3835–3840.
10. Schluck, T., Nienhaus, U., Aegerter-Wilmsen, T., and Aegerter, C.M. (2013). Mechanical control of organ size in the development of the *Drosophila* wing disc. PLoS ONE *8*, e76171.
11. Aegerter-Wilmsen, T., Aegerter, C.M., Hafen, E., and Basler, K. (2007). Model for the regulation of size in the wing imaginal disc of *Drosophila*. Mech. Dev. *124*, 318–326.
12. Legoff, L., Rouault, H., and Lecuit, T. (2013). A global pattern of mechanical stress polarizes cell divisions and cell shape in the growing *Drosophila* wing disc. Development *140*, 4051–4059.
13. Lockhart, J.A. (1965). An analysis of irreversible plant cell elongation. J. Theor. Biol. *8*, 264–275.
14. Green, P.B., and King, A. (1966). A mechanism for the origin of specifically oriented textures in development with special reference to *Nitella* wall texture. Aust. J. Biol. Sci. *19*, 421–437.
15. Williamson, R.E. (1990). Alignment of cortical microtubules by anisotropic wall stresses. Aust. J. Plant Physiol. *17*, 601–613.
16. Paredez, A.R., Somerville, C.R., and Ehrhardt, D.W. (2006). Visualization of cellulose synthase demonstrates functional association with microtubules. Science *312*, 1491–1495.
17. Baskin, T.I. (2005). Anisotropic expansion of the plant cell wall. Annu. Rev. Cell Dev. Biol. *21*, 203–222.
18. Landrein, B., and Hamant, O. (2013). How mechanical stress controls microtubule behavior and morphogenesis in plants: history, experiments and revisited theories. Plant J. *75*, 324–338.
19. Sampathkumar, A., Krupinski, P., Wightman, R., Milani, P., Berquand, A., Boudaoud, A., Hamant, O., Jönsson, H., and Meyerowitz, E.M. (2014). Subcellular and supracellular mechanical stress prescribes cytoskeleton behavior in *Arabidopsis* cotyledon pavement cells. eLife *3*, e01967.
20. Barbier de Reuille, P., Routier-Kierzkowska, A.-L., Kierzkowski, D., Bassel, G.W., Schüpbach, T., Tauriello, G., Bajpai, N., Strauss, S., Weber, A., Kiss, A., et al. (2015). MorphoGraphX: a platform for quantifying morphogenesis in 4D. eLife *4*, 05864.
21. Tauriello, G., Meyer, H.M., Smith, R.S., Koumoutsakos, P., and Roeder, A.H.K. (2015). Variability and constancy in cellular growth of *Arabidopsis* sepals. Plant Physiol. *169*, 2342–2358.
22. Smyth, D.R., Bowman, J.L., and Meyerowitz, E.M. (1990). Early flower development in *Arabidopsis*. Plant Cell *2*, 755–767.
23. Shaw, S.L. (2013). Reorganization of the plant cortical microtubule array. Curr. Opin. Plant Biol. *16*, 693–697.
24. Wasteneys, G.O., and Ambrose, J.C. (2009). Spatial organization of plant cortical microtubules: close encounters of the 2D kind. Trends Cell Biol. *19*, 62–71.
25. Lloyd, C. (2011). Dynamic microtubules and the texture of plant cell walls. Int. Rev. Cell Mol. Biol. *287*, 287–329.
26. Jacques, E., Verbelen, J.-P., and Vissenberg, K. (2013). Mechanical stress in *Arabidopsis* leaves orients microtubules in a 'continuous' supracellular pattern. BMC Plant Biol. *13*, 163.
27. Creff, A., Brocard, L., and Ingram, G. (2015). A mechanically sensitive cell layer regulates the physical properties of the *Arabidopsis* seed coat. Nat. Commun. *6*, 6382.
28. Bassel, G.W., Stamm, P., Mosca, G., Barbier de Reuille, P., Gibbs, D.J., Winter, R., Janka, A., Holdsworth, M.J., and Smith, R.S. (2014). Mechanical constraints imposed by 3D cellular geometry and arrangement modulate growth patterns in the *Arabidopsis* embryo. Proc. Natl. Acad. Sci. USA *111*, 8685–8690.
29. Uyttewaal, M., Burian, A., Alim, K., Landrein, B., Borowska-Wykręt, D., Dedieu, A., Peaucelle, A., Ludynia, M., Traas, J., Boudaoud, A., et al. (2012). Mechanical stress acts via katanin to amplify differences in growth rate between adjacent cells in *Arabidopsis*. Cell *149*, 439–451.
30. Buschmann, H., Fabri, C.O., Hauptmann, M., Hutzler, P., Laux, T., Lloyd, C.W., and Schäffner, A.R. (2004). Helical growth of the *Arabidopsis* mutant tortifolia1 reveals a plant-specific microtubule-associated protein. Curr. Biol. *14*, 1515–1521.
31. Shoji, T., Narita, N.N., Hayashi, K., Asada, J., Hamada, T., Sonobe, S., Nakajima, K., and Hashimoto, T. (2004). Plant-specific microtubule-associated protein SPIRAL2 is required for anisotropic growth in *Arabidopsis*. Plant Physiol. *136*, 3933–3944.
32. Wightman, R., Chomicki, G., Kumar, M., Carr, P., and Turner, S.R. (2013). SPIRAL2 determines plant microtubule organization by modulating microtubule severing. Curr. Biol. *23*, 1902–1907.
33. Sambade, A., Pratap, A., Buschmann, H., Morris, R.J., and Lloyd, C. (2012). The influence of light on microtubule dynamics and alignment in the *Arabidopsis* hypocotyl. Plant Cell *24*, 192–201.
34. Atkinson, S., Kirik, A., and Kirik, V. (2014). Microtubule array reorientation in response to hormones does not involve changes in microtubule nucleation modes at the periclinal cell surface. J. Exp. Bot. *65*, 5867–5875.
35. Zhang, Q., Fishel, E., Bertroche, T., and Dixit, R. (2013). Microtubule severing at crossover sites by katanin generates ordered cortical microtubule arrays in *Arabidopsis*. Curr. Biol. *23*, 2191–2195.
36. Vineyard, L., Elliott, A., Dhingra, S., Lucas, J.R., and Shaw, S.L. (2013). Progressive transverse microtubule array organization in hormone-induced *Arabidopsis* hypocotyl cells. Plant Cell *25*, 662–676.

37. Cui, M.-L., Copsey, L., Green, A.A., Bangham, J.A., and Coen, E. (2010). Quantitative control of organ shape by combinatorial gene activity. PLoS Biol. *8*, e1000538.

38. Green, A.A., Kennaway, J.R., Hanna, A.I., Bangham, J.A., and Coen, E. (2010). Genetic control of organ shape and tissue polarity. PLoS Biol. *8*, e1000537.

39. Burian, A., Ludynia, M., Uyttewaal, M., Traas, J., Boudaoud, A., Hamant, O., and Kwiatkowska, D. (2013). A correlative microscopy approach relates microtubule behaviour, local organ geometry, and cell growth at the *Arabidopsis* shoot apical meristem. J. Exp. Bot. *64*, 5753–5767.

40. Couturier, E., Courrech du Pont, S., and Douady, S. (2009). A global regulation inducing the shape of growing folded leaves. PLoS ONE *4*, e7968.

41. Couturier, E., du Pont, S.C., and Douady, S. (2011). The filling law: a general framework for leaf folding and its consequences on leaf shape diversity. J. Theor. Biol. *289*, 47–64.

42. Couturier, E., Brunel, N., Douady, S., and Nakayama, N. (2012). Abaxial growth and steric constraints guide leaf folding and shape in *Acer pseudoplatanus*. Am. J. Bot. *99*, 1289–1299.

43. Théry, M., Jiménez-Dalmaroni, A., Racine, V., Bornens, M., and Jülicher, F. (2007). Experimental and theoretical study of mitotic spindle orientation. Nature *447*, 493–496.

44. Minc, N., Burgess, D., and Chang, F. (2011). Influence of cell geometry on division-plane positioning. Cell *144*, 414–426.

45. Houk, A.R., Jilkine, A., Mejean, C.O., Boltyanskiy, R., Dufresne, E.R., Angenent, S.B., Altschuler, S.J., Wu, L.F., and Weiner, O.D. (2012). Membrane tension maintains cell polarity by confining signals to the leading edge during neutrophil migration. Cell *148*, 175–188.

46. Dalous, J., Burghardt, E., Müller-Taubenberger, A., Bruckert, F., Gerisch, G., and Bretschneider, T. (2008). Reversal of cell polarity and actin-myosin cytoskeleton reorganization under mechanical and chemical stimulation. Biophys. J. *94*, 1063–1074.

47. Verkhovsky, A.B., Svitkina, T.M., and Borisy, G.G. (1999). Self-polarization and directional motility of cytoplasm. Curr. Biol. *9*, 11–20.

48. Engler, A.J., Sen, S., Sweeney, H.L., and Discher, D.E. (2006). Matrix elasticity directs stem cell lineage specification. Cell *126*, 677–689.

49. Swift, J., and Discher, D.E. (2014). The nuclear lamina is mechano-responsive to ECM elasticity in mature tissue. J. Cell Sci. *127*, 3005–3015.

50. Lynch, T.M., and Lintilhac, P.M. (1997). Mechanical signals in plant development: a new method for single cell studies. Dev. Biol. *181*, 246–256.

51. Lecuit, T., Lenne, P.-F., and Munro, E. (2011). Force generation, transmission, and integration during cell and tissue morphogenesis. Annu. Rev. Cell Dev. Biol. *27*, 157–184.

52. Collinet, C., Rauzi, M., Lenne, P.-F., and Lecuit, T. (2015). Local and tissue-scale forces drive oriented junction growth during tissue extension. Nat. Cell Biol. *17*, 1247–1258.

53. Aigouy, B., Farhadifar, R., Staple, D.B., Sagner, A., Röper, J.-C., Jülicher, F., and Eaton, S. (2010). Cell flow reorients the axis of planar polarity in the wing epithelium of *Drosophila*. Cell *142*, 773–786.

54. Pouille, P.-A., Ahmadi, P., Brunet, A.-C., and Farge, E. (2009). Mechanical signals trigger myosin II redistribution and mesoderm invagination in *Drosophila* embryos. Sci. Signal. *2*, ra16.

55. Sherrard, K., Robin, F., Lemaire, P., and Munro, E. (2010). Sequential activation of apical and basolateral contractility drives ascidian endoderm invagination. Curr. Biol. *20*, 1499–1510.

56. Brunet, T., Bouclet, A., Ahmadi, P., Mitrossilis, D., Driquez, B., Brunet, A.-C., Henry, L., Serman, F., Béalle, G., Ménager, C., et al. (2013). Evolutionary conservation of early mesoderm specification by mechanotransduction in Bilateria. Nat. Commun. *4*, 2821.

57. Heckel, E., Boselli, F., Roth, S., Krudewig, A., Belting, H.-G., Charvin, G., and Vermot, J. (2015). Oscillatory flow modulates mechanosensitive klf2a expression through trpv4 and trpp2 during heart valve development. Curr. Biol. *25*, 1354–1361.

58. Zhang, H., Landmann, F., Zahreddine, H., Rodriguez, D., Koch, M., and Labouesse, M. (2011). A tension-induced mechanotransduction pathway promotes epithelial morphogenesis. Nature *471*, 99–103.

59. Farge, E. (2003). Mechanical induction of Twist in the *Drosophila* foregut/stomodeal primordium. Curr. Biol. *13*, 1365–1377.

60. Desprat, N., Supatto, W., Pouille, P.-A., Beaurepaire, E., and Farge, E. (2008). Tissue deformation modulates twist expression to determine anterior midgut differentiation in *Drosophila* embryos. Dev. Cell *15*, 470–477.

61. Vlad, D., Kierzkowski, D., Rast, M.I., Vuolo, F., Dello Ioio, R., Galinha, C., Gan, X., Hajheidari, M., Hay, A., Smith, R.S., et al. (2014). Leaf shape evolution through duplication, regulatory diversification, and loss of a homeobox gene. Science *343*, 780–783.

62. Ueda, K., Matsuyama, T., and Hashimoto, T. (1999). Visualization of microtubules in living cells of transgenic *Arabidopsis thaliana*. Protoplasma *206*, 201–206.

63. Bichet, A., Desnos, T., Turner, S., Grandjean, O., and Höfte, H. (2001). BOTERO1 is required for normal orientation of cortical microtubules and anisotropic cell expansion in *Arabidopsis*. Plant J. *25*, 137–148.

64. Hamant, O., Das, P., and Burian, A. (2014). Time-lapse imaging of developing meristems using confocal laser scanning microscope. Methods Mol. Biol. *1080*, 111–119.

65. Bonazzi, D., Julien, J.-D., Romao, M., Seddiki, R., Piel, M., Boudaoud, A., and Minc, N. (2014). Symmetry breaking in spore germination relies on an interplay between polar cap stability and spore wall mechanics. Dev. Cell *28*, 534–546.

66. Hecht, F. (2012). New development in freefem++. J. Numer. Math. *20*, 251–266.

67. Bozorg, B., Krupinski, P., and Jönsson, H. (2014). Stress and strain provide positional and directional cues in development. PLoS Comput. Biol. *10*, e1003410.